Shape from Shading for Rough Surfaces: Analysis of the Oren-Nayar Model

Yong Chul Ju
y.ju@mmci.uni-saarland.de

Michael Breuß
breuss@tu-cottbus.de

Andrés Bruhn
bruhn@vis.uni-stuttgart.de

Silvano Galliani
galliani@mia.uni-saarland.de

Vision and Image Processing Group
Saarland University, Germany

Institute for Applied Mathematics and Scientific
Computing, BTU Cottbus, Germany

Institute for Visualization and Interactive Systems
University of Stuttgart, Germany

Mathematical Image Analysis Group
Saarland University, Germany

Abstract

Due to their improved capability to handle realistic illumination scenarios, non-Lambertian reflectance models are becoming increasingly more popular in the Shape from Shading (SfS) community. One of these advanced models is the *Oren-Nayar* model which is particularly suited to handle rough surfaces. However, not only the proper selection of the model is important, also the validation of *stable* and *efficient* algorithms plays a fundamental role when it comes to the practical applicability. While there are many works dealing with such algorithms in the case of Lambertian SfS, no such analysis has been performed so far for the Oren-Nayar model. In our paper we address this problem and present an in-depth study for such an advanced SfS model. To this end, we investigate under which conditions, i.e. model parameters, the Fast Marching (FM) method can be applied – a method that is known to be one of the most efficient algorithms for solving the underlying partial differential equations of Hamilton-Jacobi type. In this context, we do not only perform a *general* investigation of the model using Osher's criterion for verifying the suitability of the FM method. We also conduct a *parameter dependent* analysis that shows, that FM can safely be used for the model for a wide range of settings relevant for practical applications. Thus, for the first time, it becomes possible to *theoretically justify* the use of the FM method as solver for the Oren-Nayar model which has been applied so far on a purely empirical basis only. Numerical experiments demonstrate the validity of our theoretical analysis. They show a stable behaviour of the FM method for the predicted range of model parameters.

1 Introduction

Since almost five decades *Shape from Shading (SfS)* is one of the fundamental problems in computer vision. Having many interesting applications such as astronomy [17], terrain reconstruction [4], endoscopy [21, 27] or dentistry [1], the goal of SfS is to recover the surface of an object from a single input image under the assumption that a reflectance model and the light information are available. For a long time, the research in SfS was mainly dominated

by approaches based on relatively simple model assumptions such as an orthographic camera setup and a Lambertian surface model [7, 8, 28]. Not surprisingly, results were often rather limited in terms of quality or approaches even failed in practice, *e.g.* for realistic imagery. However, recently, more realistic concepts such as *perspective cameras* [14, 15, 21] and *non-Lambertian reflectance models* [3, 19] found their way into research and led to considerable progress in the field. In particular, considering more realistic camera models *and* more realistic reflectance models combined with a physically motivated *light attenuation term* [15] turned out to be useful from both a theoretical and practical viewpoint [2, 25].

In this context, the *Oren-Nayar* reflectance model [10, 11, 12] seems to be a very appealing choice. Based on the microfacet approach of Torrance and Sparrow [22] it allows to model rough materials realistically whose surface properties are considerably different from those of Lambertian surfaces. Such non-Lambertian materials are *e.g.* concrete, plaster, clay or cloth. However, there is a price to pay when considering such advanced SfS models:

(i) On the one hand, a theoretical analysis of the model becomes much more difficult. While for the Lambertian case Prados and Faugeras [15] were able to show that combining the assumption of a projective camera with a light attenuation term may turn the originally ill-posed SfS problem into a partially well-posed one (cf. [6]), no such thorough analysis has been performed for the advanced Oren-Nayar model so far. Moreover, to the best of our knowledge, there is only one work in the entire literature that presents such an in-depth study for a modern non-Lambertian SfS model: In [5], Breuß and Ju investigate important issues such as critical points and convexity in the context of SfS with the Phong model [25].

(ii) On the other hand, deriving suitable computational methods for solving the underlying mathematical equations - nonlinear PDEs of Hamilton-Jacobi type – becomes a highly challenging task. Moreover, issues like efficiency play a very important role when it comes to the practical applicability. Hence, in the context of non-Lambertian SfS, Ahmed and Farag [2] first proposed a solver based on a Lax-Friedrichs sweeping scheme [9] under the general assumption that the model described by the Hamilton-Jacobi equation is non-convex. While this scheme offers a broad applicability, it is known to be extremely slow in practice. Consequently, as an alternative in the context of SfS with the Phong model, Vogel et. al. [26] proposed a solution based on the popular fast marching (FM) method [20]. This approach was later on generalised by Vogel and Cristiani [24] to other non-Lambertian SfS models including the Oren-Nayar model. However, although the FM method was able to achieve huge speedups of *up to factor 100* compared to the Lax-Friedrichs scheme, no theoretical justification was given why the proposed algorithm works for the considered cases. In particular, no analysis in terms of *Osher's criterion* [13, 16, 23] was conducted which allows to decide if the FM method can be applied for solving a certain Hamilton-Jacobi equation, even if the underlying model is non-convex.

Summarising, the Oren-Nayar SfS model is promising but challenging at the same time: So far there is no theoretical basis for using efficient algorithms such as the FM method and it is completely unclear under which model parameters they can be applied.

In this paper we address both problems by presenting the first in-depth analysis of the Oren-Nayar SfS model in the literature. By analysing this model with respect to Osher's criterion we shed light on its properties – in particular on its behaviour depending on the model parameters. Our contributions are twofold: (i) We provide the range of the roughness parameter under which Osher's criterion is always valid. Thus, for the first time, it becomes possible to give a theoretical justification for applying the FM method for solving the Oren-Nayar SfS model. In this context, we also succeed in validating the empirical parameter findings from [24]. (ii) We provide an additional parameter dependent analysis which allows

to broaden the range of theoretically justified applications even further. Summarising, we put the application of the FM method for solving the Oren-Nayar method on a solid theoretical basis and give clear requirements when this efficient solver can be used safely in practice.

The paper is organised as follows. In Section 2, we briefly review the Oren-Nayar surface reflectance model and derive the corresponding SfS approach. Then, in Section 3, we investigate the behaviour of this approach with respect to Osher's criterion – first in 1-D and then in 2-D. Thereafter, we present numerical experiments in Section 4 that confirm our theoretical findings. Finally, the paper ends with a conclusion in Section 5.

2   Shape from Shading with the Oren-Nayar Model

In this section we will first review the Oren-Nayar surface reflectance model and then describe the corresponding SfS approach based on that model. This will provide us with the required mathematical basis for our detailed model analysis in Section 3.

Oren-Nayar Reflectance Model. The Oren-Nayar surface reflectance model [10, 11, 12] has been primarily designed for handling rough surfaces by aggregating many Lambertian surface patches, see Figure 1. The roughness is characterised by a Gaussian probability distribution of the facet slopes with standard deviation (roughness parameter) $\sigma \in [0, \frac{\pi}{2}]$. If $\sigma = 0$, the surface does not exhibit any slopes and the Oren-Nayar model collapses to the Lambertian case. The main idea of Oren-Nayar is to compute the radiance contributed from all individual facets on a given surface patch. The total irradiance of such a patch is then determined by adding the contributions of all facets, cf. [10] for details on the derivation.

Figure 1: Illustration of the cross section of a patch dA in the Oren-Nayar model. One patch is composed of many symmetric V-shape cavities and two facets comprise one V-cavity. Each facet is assumed to be Lambertian and very small compared to the whole patch dA.
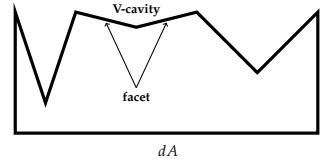
Oren-Nayar SfS.   Assuming the facets to be Gaussian distributed as mentioned above and considering an additional light attenuation term $1/r^2$ that models the inverse square law known from light transport, the final brightness equation for *all facets* of the Oren-Nayar surface reflectance model can be summarised as [2]:

$$I = \frac{1}{r^2} \frac{\rho}{\pi} L_i \cos \theta_i \left(A + B \sin \alpha \tan \beta \max(0, \cos(\phi_r - \phi_i)) \right), \qquad (1)$$

where the facet statistics enters the model in terms of the two factors

$$A = 1 - 0.5 \frac{\sigma^2}{\sigma^2 + 0.33} \qquad \text{and} \qquad B = 0.45 \frac{\sigma^2}{\sigma^2 + 0.09} \geq 0. \qquad (2)$$

In this context, ρ denotes the surface albedo, L_i is the intensity of the point light source, θ_i represents the angle between the surface normal and light source direction, θ_r stands for the angle between the surface normal and camera direction, ϕ_i is the angle between the light source and the reference direction on the surface, ϕ_r denotes the angle between the camera and the reference direction on the surface, and the two variables $\alpha = \max(\phi_i, \phi_r)$, $\beta = \min(\phi_i, \phi_r)$ stand for the maximum and minimum of the angles ϕ_i and ϕ_r, respectively. An overview of all the different angles occurring in the Oren-Nayar model is given in Figure 2.
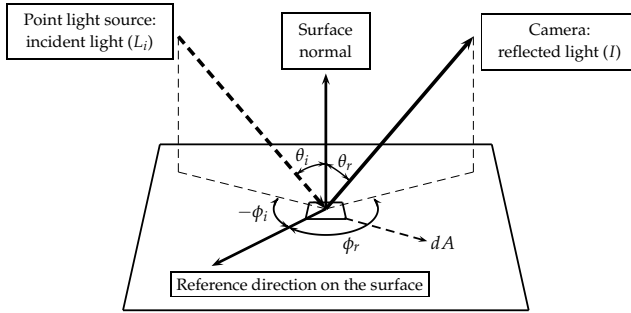
Figure 2: Illustration of diffuse reflectance parameters for SfS with Oren-Nayar reflectance. *dA* denotes a patch shown in Figure 1.

To obtain a more tractable model, we follow the idea from [2] and assume that the factor $\frac{\rho}{\pi}L_i$ in Eq. (1) is known to be 1 and that the point light source L_i is located at the optical centre of the camera. This yields $\alpha = \beta = \theta_i = \theta_r = \theta$ and $\phi_r - \phi_i = 0$. Moreover, as shown in [15] we can parametrise the unknown surface $\mathcal{S}$ under a projective camera model via

$$\mathcal{S} = \left\{ \frac{\mathtt{f}}{\sqrt{|\mathbf{x}|^2 + \mathtt{f}^2}} u(x_1, x_2) \begin{bmatrix} x_1 \\ x_2 \\ -\mathtt{f} \end{bmatrix} \middle| \mathbf{x} := (x_1, x_2)^T \in \overline{\Omega} \right\}, \quad \mathcal{S} : \Omega \to \mathbb{R}^3, \qquad (3)$$

where $u(x_1, x_2)$ denotes the unknown depth from the camera centre in multiples of the focal length $\mathtt{f}$ and $\Omega \subset \mathbb{R}^2$ represents the image plane. We can then compute the surface normal via $\mathcal{S}_{x_1} \times \mathcal{S}_{x_2}$ and rewrite the expression $\cos \theta_i$ in Eq. (1) as scalar product between the light direction and this surface normal. As a result, the original equation in (1) simplifies to the Oren-Nayar SfS model proposed by Ahmed and Farag [2]:

$$H_{2D} = \mathtt{f}^2 I \frac{M+1}{A\sqrt{M+1} + BM} - e^{-2v} = 0 \qquad (4)$$

where

$$M = \left[\mathtt{f}^2 |\nabla v(\mathbf{x})|^2 + (\nabla v(\mathbf{x}) \cdot \mathbf{x})^2 \right] \left(\frac{|\mathbf{x}|^2 + \mathtt{f}^2}{\mathtt{f}^2} \right). \qquad (5)$$

The so-called Hamiltonian H_{2D} of the Oren-Nayar SfS model is expressed in terms of the *logarithm* of the depth u denoted by $v = \ln u$. This step is typically performed to eliminate some nonlinear expressions which facilitates our analysis in Section 3. For a more detailed derivation of the Hamiltonian in Eq. (4) we refer the reader to [2].

3   Theoretical Analysis

There is a variety of methods to solve PDEs of Hamilton-Jacobi type such as (4). One of the most efficient algorithms in this context is the FM method [20] that reconstructs the entire surface by propagating depth information from one or more starting points with known depth. Typically, so-called *critical points* of an object surface are chosen for this purpose, i.e. points that are locally of minimal distance to the camera. Since in the considered model

the light source is located in the camera centre, such points can be easily identified by their maximal brightness. However, it is important for FM that the depth can only be computed from foreground to background. The main reason for this comes from the nature of the *upwind-type scheme* [18] that is used in the FM method for discretising the partial derivatives. Since the upwind scheme locally selects the direction for computing the derivatives, the FM method must consider this direction when propagating the information from the starting point to the remaining surface. On the other hand, for non-convex models this way to perform computations is in general not correct anyway.

Osher's Criterion. In [13], Osher elaborated on this requirement and formulated the following sufficient condition for the applicability of the FM method:

$$p[H_{2D}]_p \geq 0, \quad q[H_{2D}]_q \geq 0, \tag{6}$$

where $p = \frac{\partial v}{\partial x_1}$ and $q = \frac{\partial v}{\partial x_2}$. It basically states that partial derivatives of the unknown function, in our case v, and the corresponding directions of the upwind scheme have the same sign. If this so-called *Osher's criterion* is fulfilled, one can apply the FM method irrespectively of the convexity of the underlying Hamiltonian H_{2D} [13]. This criterion forms the basis of our investigation of the Oren-Nayar model in 1D and 2D.

3.1 One-dimensional Case

Actually, there are three variables appearing in Eq. (4) except the unknown function v: the pixel position $\mathbf{x}$ and the two model parameters given by σ and $\mathtt{f}$ for the surface roughness and the focal length, respectively. Hence, in order to investigate the role of σ, we first perform a general analysis and consider the Oren-Nayar model with arbitrary focal length. Then, we conduct an extended parameter dependent analysis for models with a specific focal length.

General Analysis. Following Eq. (4) and defining $p := v'$ gives us the 1D Hamiltonian

$$H_{1D} = \mathtt{f}^2 I \frac{M_{1D}+1}{A\sqrt{M_{1D}+1}+BM_{1D}} - e^{-2v}, \tag{7}$$

where

$$M_{1D} := \left[\mathtt{f}^2 p^2 + p^2 x_1^2\right] \left(\frac{|x_1|^2 + \mathtt{f}^2}{\mathtt{f}^2}\right). \tag{8}$$

Accordingly, Osher's criterion in Eq. (6) reads in the 1D case

$$p[H_{1D}]_p \geq 0. \tag{9}$$

Applying this criterion to our model and using standard quotient and chain rules yields

$$p^2 \frac{\mathtt{f}^2 I W_{1D} Q_{1D}}{D_{1D}} \underbrace{\left[2 - \frac{(M_{1D}+1)}{D_{1D}}\left(\frac{A}{\sqrt{M_{1D}+1}} + 2B\right)\right]}_{=:\Psi} \geq 0, \tag{10}$$

where $D_{1D} := A\sqrt{M_{1D}+1}+BM_{1D}$, $W_{1D} := \mathtt{f}^2 + x_1^2$ and $Q_{1D} := (x_1^2 + \mathtt{f}^2)/\mathtt{f}^2$. Since we have by construction that $\mathtt{f}^2, I, W_{1D}, Q_{1D}, D_{1D} > 0$ holds, this comes down to

$$p^2\Psi \geq 0 \iff \Psi \geq 0 \iff 2 \geq \frac{(M_{1D}+1)}{D_{1D}}\left(\frac{A}{\sqrt{M_{1D}+1}} + 2B\right). \tag{11}$$

Some straightforward algebraic manipulations further yield

$$A\sqrt{M_{1D}+1} - 2B \geq 0 \tag{12}$$

from which we can then conclude

$$A\sqrt{M_{1D}+1} \geq 2B \;\Rightarrow\; A^2(M_{1D}+1) \geq 4B^2 \;\Rightarrow\; M_{1D} \geq \frac{4B^2 - A^2}{A^2}. \tag{13}$$

By the non-negativity of M_{1D} we can finally derive the following *sufficient condition* for the validity of Osher's criterion:

$$4B^2 - A^2 \leq 0 \;\Leftrightarrow\; A \geq 2B. \tag{14}$$

Range of the Roughness Parameter. Since A and B in (14) are functions of the roughness parameter σ, it is even possible to go one step further. We can explicitly state the range of σ for which Osher's criterion is valid. Plugging Eq. (2) into Eq. (14) gives first

$$\left(1 - 0.5\frac{\sigma^2}{\sigma^2+0.33}\right) \geq 2\left(0.45\frac{\sigma^2}{\sigma^2+0.09}\right) \tag{15}$$
$$\Rightarrow\; 0.4\sigma^4 - 0.078\sigma^2 - 0.0297 \leq 0.$$

Substituting $\gamma := \sigma^2 \geq 0$ in Eq. (15) and solving the corresponding inequality then yields

$$0 \leq \gamma < 0.3869067207 \;\Rightarrow\; 0 \leq \sigma < \sqrt{0.3869067207} \approx 0.622. \tag{16}$$

Let us summarise this fundamental result:

Theorem 1

> For the Oren-Nayar SfS model given by (4) with arbitrary focal length $\mathtt{f}$, Osher's criterion is always satisfied if the roughness parameter σ is in the range specified in (16).

Parameter Dependent Analysis. So far we have conducted a general investigation of the Oren-Nayar SfS model that is valid independently of the actual value of the focal length $\mathtt{f}$. In the following we perform an extended analysis using Osher's criterion that depends on the concrete value of $\mathtt{f}$. This allows us to refrain from using the cautious estimate $M_{1D} \geq 0$ in the step from (13) to (14). Instead we use the actual definition of M_{1D} given by (8), but consider the case $x = 0$. As one can verify, this strategy gives us the lower bound for M_{1D} with respect to all values of x. This fits also nicely to the classic assumption in SfS that the object of interest is located at the centre of the input image. We thus obtain

$$M_{1D} = p^2\mathtt{f}^2. \tag{17}$$

By combining the result of (13) and (17), we are able to extract the *tighter condition*

$$|p|^2\mathtt{f}^2 \geq \frac{4B^2 - A^2}{A^2} \;\Rightarrow\; |p|^2 \geq \frac{4B^2 - A^2}{A^2\mathtt{f}^2} =: \Upsilon(\sigma,\mathtt{f}). \tag{18}$$

Interpretation. The tighter condition in Eq. (18) tells us two things: (i) Osher's criterion is always fulfilled if the variation $|p| = |v'|$ of the surface $\mathcal{S}$ is sufficiently large. In other words: "We are away from critical points". (ii) Potential problems may only occur at and
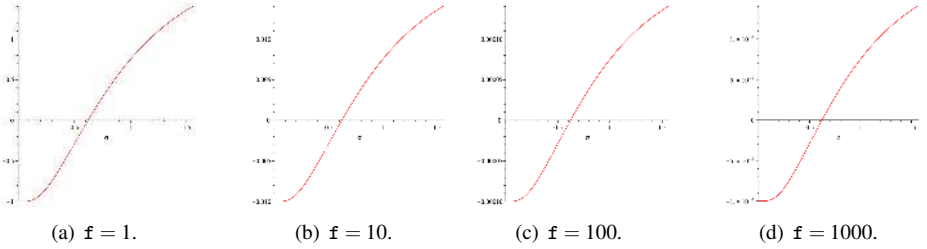
(a) $\mathtt{f} = 1$. (b) $\mathtt{f} = 10$. (c) $\mathtt{f} = 100$. (d) $\mathtt{f} = 1000$.

Figure 3: Plots of the function $\Upsilon(\sigma, \mathtt{f})$ for different values of $\mathtt{f}$. It is important to note that for each focal length $\mathtt{f}$ the scale of the values for Υ is very different.

around critical points, i.e. where $|p|$ is zero or very small. Note that points with $p = 0$ are of no concern, since the PDE can be solved analytically in this case. Exactly this is done when initialising depth values at critical points before using the FM scheme.

What remains to be considered is the situation for small values of $|p|$, in order to investigate remaining potential problems. To this end, in Figure 3, we have plotted the graph of the function Υ depending on $\sigma \in [0, \frac{\pi}{2}]$ for different values of the focal length $\mathtt{f}$. Again, we can observe two findings: (i) The graphs confirm our result from the general analysis: For the corresponding range of σ in (16), all functions are negative and thus the tighter condition in (18) holds independently of the focal length. (ii) For typical cameras with focal length $\mathtt{f} = \mathcal{O}(10^2)$, the function values of Υ that correspond to values of σ outside the range in (16) are positive but negligibly small. This shows that the tighter condition holds already for surfaces with slight depth variations – independently of a violation of the sufficient condition.

Remark 1

> *A violation of the sufficient condition on the roughness parameter σ is not of practical relevance, since in general, for typical cameras with focal length $\mathtt{f} = \mathcal{O}(10^2)$ and surfaces with slight depth variations, the tighter condition will be fulfilled anyway.*

3.2 Two-dimensional Case

The analysis in the 2D case is based on Eq. (4) and Eq. (5) and proceeds analogously to that of the 1D case. Defining $p := v_x$ and $q := v_y$, we finally obtain the following two criteria:

$$p[H_{2D}]_p = \frac{\left[p^2(\mathtt{f}^2 + x_1^2) + pqx_1x_2\right]Q_{2D}}{D_{2D}^2}\left(A\sqrt{M_{2D}+1} - 2B\right) \geq 0, \tag{19a}$$

$$q[H_{2D}]_q = \frac{\left[q^2(\mathtt{f}^2 + x_2^2) + pqx_1x_2\right]Q_{2D}}{D_{2D}^2}\left(A\sqrt{M_{2D}+1} - 2B\right) \geq 0, \tag{19b}$$

where $D_{2D} := A\sqrt{M_{2D}+1} + BM_{2D}$, $W_{2D} := \mathtt{f}^2 + x_1^2 + x_2^2$ and $Q_{2D} := (x_1^2 + x_2^2 + \mathtt{f}^2)/\mathtt{f}^2$. Since (19a) and (19b) have the same structure, it suffices to discuss (19a) in detail. Evidently, our findings can then be extended to (19b) accordingly.

First, we note that we have already discussed a factor of the form $\left(A\sqrt{M_* + 1} - 2B\right)$ in both the general and the parameter dependent analysis of the 1-D case; see Eq. (12). Thus we can take over the corresponding results. Moreover, we know that $Q_{2D}, D_{2D} > 0$. Consequently, it remains to analyse for which conditions the following inequality holds:

$$p^2(\mathtt{f}^2 + x_1^2) + pqx_1x_2 \geq 0 \tag{20}$$

Since the first term in (20) is non-negative by construction, we only have to check the second term. For an estimate of pqx_1x_2, one can think of four possible cases

$$
\begin{array}{lll}
\text{(i)} & |p| \geq |q| \text{ and } |x_1| \geq |x_2| & \Rightarrow \quad pqx_1x_2 \geq -p^2x_1^2 \\
\text{(ii)} & |p| \geq |q| \text{ and } |x_2| \geq |x_1| & \Rightarrow \quad pqx_1x_2 \geq -p^2x_2^2 \\
\text{(iii)} & |q| \geq |p| \text{ and } |x_1| \geq |x_2| & \Rightarrow \quad pqx_1x_2 \geq -q^2x_1^2 \\
\text{(iv)} & |q| \geq |p| \text{ and } |x_2| \geq |x_1| & \Rightarrow \quad pqx_1x_2 \geq -q^2x_2^2 .
\end{array}
\tag{21}
$$

By considering each case in (21), we can derive the following conditions from (20):

$$
\begin{array}{lll}
\text{(i)} & p^2(\mathtt{f}^2+x_1^2) - p^2x_1^2 \geq 0 & \Rightarrow \quad p^2\mathtt{f}^2 \geq 0 \\[4pt]
\text{(ii)} & p^2(\mathtt{f}^2+x_1^2) - p^2x_2^2 \geq 0 & \Rightarrow \quad \mathtt{f}^2 \geq x_2^2 - x_1^2 \\[4pt]
\text{(iii)} & p^2(\mathtt{f}^2+x_1^2) - q^2x_1^2 \geq 0 & \Rightarrow \quad \mathtt{f}^2 \geq \dfrac{q^2-p^2}{p^2}x_1^2 \\[8pt]
\text{(iv)} & p^2(\mathtt{f}^2+x_1^2) - q^2x_2^2 \geq 0 & \Rightarrow \quad \mathtt{f}^2 \geq \dfrac{q^2}{p^2}x_2^2 .
\end{array}
\tag{22}
$$

In view of (22) and the corresponding conditions for q, we can derive the following theorem:

Theorem 2

For the 2D case of the Oren-Nayar SfS model, Osher's critertion is satisfied if the tighter condition in (18) is fulfilled and additionally $\mathtt{f}^2 \geq \max(\frac{q^2}{p^2}, \frac{p^2}{q^2}) \max(|x_1|^2, |x_2|^2)$ holds.

Remark 2

Although the factor $\max(\frac{q^2}{p^2}, \frac{p^2}{q^2})$ in Theorem 2 may theoretically represent a potential difficulty for one large and one small value of p and q, respectively, there is no problem in practice for smooth surfaces, since such cases only occur at strong discontinuities.

In [24], Vogel and Cristiani used a value of $\sigma = 0.5$ for the roughness parameter in the Oren-Nayar SfS model. Based on Theorem 1 and 2 we can theoretically justify that the FM method is an adequate numerical solver for this parameter setting, i.e. for their specific model.

4   Numerical Experiments

Let us now investigate the performance of the FM method for the Oren-Nayar SfS model by means of two experiments. In our first experiment we rendered a *Sphere* for a focal length of $\mathtt{f} = 128$ and a roughness parameter of $\sigma = \frac{\pi}{2}$. The corresponding input image depicted in Figure 4(a) has a size of 256×256. If we compare the ground truth in Figure 4(b) and the computed result in Figure 4(c), we can clearly see that the FM method has problems in practice for such model settings. In particular close to the critical point at the centre of the input image the reconstruction appears to be significantly too flat. This confirms our findings from the theoretical analysis that for large values of σ, regions close to critical points can pose problems if the variation of the depth is too small (Theorem 1, Remark 1).

In our second experiment, we use the same settings, but consider a much more challenging input image: the *Mozart* face. Moreover, we computed an additional rendering for a roughness parameter of $\sigma = 0.5$ which is clearly in the range of admitted parameters for the
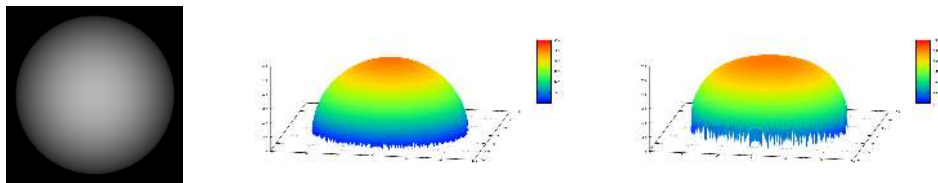
(a) Input image $\sigma = \frac{\pi}{2}$.   (b) Sphere ground truth for $f = 128$.   (c) Reconstruction of Figure 4(a).

Figure 4: The Sphere Experiment.

sufficient condition in Eq. (16). If we take a look at the results in Figure 5(d) and 5(e), the difference between both parameter settings become obvious. As one can see, the FM method works reasonably well in practice for a roughness parameter of $\sigma = 0.5$. In particular, one cannot observe too much distortion as slopes have a realistically large variation. In contrast, the result for $\sigma = \frac{\pi}{2}$ looks really poor. Here, one can clearly see that at locations close to strong discontinuities, the FM method runs into problems (*e.g.* at the eyebrows). Once again, this confirms our findings from the theoretical analysis (Theorem 2, Remark 2).

(a) Input image with $\sigma = 0.5$.   (b) Input image with $\sigma = \frac{\pi}{2}$.   (c) Mozart ground truth for $f = 128$.   (d) Reconstruction of Figure 5(a).   (e) Reconstruction of Figure 5(b).

Figure 5: The Mozart Experiment.

Finally, we would like to note that applying the FM method for the Oren-Nayar SfS model speeds up the computation from 46.3 second to 0.73 second for images of size 256×256 compared to the Lax-Friedrichs sweeping scheme; see [24]. Even larger speedups can be expected for larger input images. This demonstrates the importance for having a theoretical justification for applying the FM method with the Oren-Nayar SfS model in practice.

5 Conclusion

We have presented the first analysis of a modern Oren-Nayar SfS model showing that the highly efficient FM method can readily be applied in practical applications. We have highlighted important model properties like the dependence on the roughness parameter and the focal length, and we have identified for the first time safe parameter ranges for such a SfS model. In the course of our analysis, also a theoretical basis for the proper interpretation of computed reconstruction results is given. Thus, we believe that our work can be considered a nice example for the successful interaction of numerical analysis and computer vision.

References

[1] A.S. Abdelrahim, M.A. Abdelrahman, H. Abdelmunim, A. Farag, and M. Miller. Novel image-based 3d reconstruction of the human jaw using shape from shading and feature descriptors. In *Proceedings of the British Machine Vision Conference (BMVC)*, pages 1–11, 2011.

[2] A.H. Ahmed and A.A. Farag. A new formulation for shape from shading for non-Lambertian surfaces. In *Proc. IEEE Conference on Computer Vision and Pattern Recognition (CVPR)*, volume 2, pages 1817–1824, 2006.

[3] S. Bakshi and Y.-H. Yang. Shape from shading for non-Lambertian surfaces. In *Proc. IEEE International Conference on Image Processing (ICIP)*, volume 2, pages 130–134, 1994.

[4] A.G. Bors, E.R. Hancock, and R.C. Wilson. Terrain analysis using radar shape-from-shading. *IEEE Transactions on Pattern Analysis and Machine Intelligence*, 25(8):974–992, 2003.

[5] M. Breuß and Y.C. Ju. Shape from shading with specular highlights: Analysis of the Phong model. In *Proc. IEEE International Conference on Image Processing (ICIP)*, pages 9–12, 2011.

[6] M. Breuß, E. Cristiani, J.-D. Durou, M. Falcone, and O. Vogel. Perspective shape from shading: Ambiguity analysis and numerical approximations. *SIAM Journal on Imaging Sciences*, 5(1):311–342, 2012.

[7] J.-D. Durou, M. Falcone, and M. Sagona. Numerical methods for shape-from-shading: A new survey with benchmarks. *Computer Vision and Image Understanding*, 109(1): 22–43, 2008.

[8] B.K.P. Horn and M.J. Brooks. *Shape from Shading*. The MIT Press, 1989.

[9] C.Y. Kao, S. Osher, and J. Qian. Lax-Friedrichs sweeping scheme for static Hamilton-Jacobi equations. *Journal of Computational Physics*, 196:367–391, 2004.

[10] S.K. Nayar and M. Oren. Generalization of the Lambertian model and implications for machine vision. *International Journal of Computer Vision*, 14(3):227–251, 1995.

[11] M. Oren and S.K. Nayar. Diffuse reflectance from rough surfaces. In *Proc. IEEE Conference on Computer Vision and Pattern Recognition (CVPR)*, pages 763–764, 1993.

[12] M. Oren and S.K. Nayar. Seeing beyond Lambert's law. In *Proc. European Conference on Computer Vision (ECCV)*, volume B, pages 269–280, 1994.

[13] S. Osher. A level set formulation for the solution of the Dirichlet problem for Hamilton–Jacobi equations. *SIAM Journal on Mathematical Analysis*, 24(5):1145–1152, 1993.

[14] E. Prados and O.D. Faugeras. Perspective shape from shading and viscosity solutions. In *IEEE International Conference on Computer Vision (ICCV)*, pages 826–831, 2003.

[15] E. Prados and O.D. Faugeras. Shape from shading: a well-posed problem? In *IEEE Conference on Computer Vision and Pattern Recognition (CVPR)*, volume 2, pages 870–877, 2005.

[16] J. Qian, Y.-T. Zhang, and H.-K. Zhao. A fast sweeping method for static convex Hamilton–Jacobi equations. *Journal of Scientific Computing*, 31:237–271, 2007.

[17] T. Rindfleisch. Photometric method for lunar topography. *Photogrammetric Engineering*, 32(2):262–277, 1966.

[18] E. Rouy and A. Tourin. A viscosity solutions approach to shape-from-shading. *SIAM Journal on Numerical Analysis*, 29(3):867–884, 1992.

[19] D. Samaras and D. Metaxas. Incorporating illumination constraints in deformable models for shape from shading and light direction estimation. *IEEE Transactions on Pattern Analysis and Machine Intelligence*, 25(2):247–264, 2003.

[20] J.A. Sethian. *Level Set Methods and Fast Marching Methods*. Cambridge University Press, 2nd edition, 1999.

[21] A. Tankus, N. Sochen, and Y. Yeshurun. Perspective shape-from-shading by fast marching. In *IEEE Conference on Computer Vision and Pattern Recognition (CVPR)*, volume 1, pages 43–49, 2004.

[22] K.E. Torrance and E.M. Sparrow. Theory for off-specular reflection from roughened surfaces. *Journal of the Optical Society of America*, 57(9):1105–1114, 1967.

[23] Y.-H.R. Tsai, L.-T. Cheng, S. Osher, and H.-K. Zhao. Fast sweeping algorithms for a class of Hamilton–Jacobi equations. *SIAM Journal on Numerical Analysis*, 41(2): 673–694, 2003.

[24] O. Vogel and E. Cristiani. Numerical schemes for advanced reflectance models for shape from shading. In *Proc. IEEE International Conference on Image Processing (ICIP)*, pages 5–8, 2011.

[25] O. Vogel, M. Breuß, and J. Weickert. Perspective shape from shading with non-Lambertian reflectance. In *Proceedings of the 30th DAGM symposium on Pattern Recognition*, pages 517–526, 2008.

[26] O. Vogel, M. Breuß, T. Leichtweis, and J. Weickert. Fast shape from shading for phong-type surfaces. In *Scale Space and Variational Methods in Computer Vision*, volume 5567 of *Lecture Notes in Computer Science*, pages 733–744. Springer, 2009.

[27] C. Wu, S. Narasimhan, and B. Jaramaz. A multi-image shape-from-shading framework for near-lighting perspective endoscopes. *International Journal of Computer Vision*, 86:211–228, 2010.

[28] R. Zhang, P.-S. Tsai, J.E. Cryer, and M. Shah. Shape from shading: A survey. *IEEE Transactions on Pattern Analysis and Machine Intelligence*, 21(8):690–706, 1999.